Published in final edited form as:
Nat Commun. ; 5: 4582. doi:10.1038/ncomms5582.

Magnetic behaviour of $TbPc_2$ single-molecule magnets chemically grafted on silicon surface

Matteo Mannini[a,*], **Federico Bertani**[b], **Cristina Tudisco**[c], **Luigi Malavolti**[a], **Lorenzo Poggini**[a], **Kasjan Misztal**[b], **Daniela Menozzi**[b], **Alessandro Motta**[c], **Edwige Otero**[d], **Philippe Ohresser**[d], **Philippe Sainctavit**[d,e], **Guglielmo G. Condorelli**[c], **Enrico Dalcanale**[b], and **Roberta Sessoli**[a]

[a]Department of Chemistry "Ugo Schiff" & INSTM RU, University of Firenze, via della Lastruccia 3-13, 50019, Sesto Fiorentino, Italy

[b]Department of Chemistry, University of Parma and INSTM RU, Parco Area delle Scienze 17/A 43124 Parma, Italy

[c]Department of Chemical Science, University of Catania and INSTM RU, Viale Andrea Doria, 6, 95125 Catania, Italy

[d]Synchrotron SOLEIL, L'Orme des Merisiers Saint-Aubin - BP 48, 91192 Gif-sur-Yvette, France

[e]IMPMC-CNRS, Université Pierre et Marie Curie, 4 place Jussieu 75252 Paris Cedex 05, France

Abstract

Single-molecule magnets (SMMs) are among the most promising molecular systems for the development of novel molecular electronics based on the spin transport. Going beyond the investigations focused on physisorbed SMMs, in this work the robust grafting of Terbium(III) bis(phthalocyaninato) complexes to silicon surface from a diluted solution is achieved by rational chemical design yielding the formation of a partially oriented monolayer on the conducting substrate. Here, by exploiting the surface sensitivity of X-ray circular magnetic dichroism we evidence an enhancement of the magnetic bistability of this single-molecule magnet, in contrast to the dramatic reduction of the magnetic hysteresis that characterises monolayer deposits evaporated on noble and ferromagnetic metals. Photoelectron spectroscopy investigations and density functional theory analysis suggest a non-innocent role played by the silicon substrate, evidencing the potentiality of this approach for robust integration of bistable magnetic molecules in electronic devices.

*CORRESPONDING AUTHOR INFO: matteo.mannini@unifi.it.

CONTRIBUTIONS

M.M., R.S and E.D. designed and coordinated this study, M.M., C.T., F.B., Ph. S., R.S., G.C. and E.D. wrote the paper. F.B., K.M. and D.M. carried out the synthesis and the bulk chemical characterisation, M.M. and R.S. performed the bulk magnetic characterisation, C.T. and G.C. performed the silicon grafting; C.T., G.C., L.M., L.P. and M.M. performed the XPS characterisation; A.M. performed DFT modelling, M.M., Ph.S., L.M., L.P., E.O. and Ph. O. carried out the synchrotron experiments. All authors commented on the manuscript.

COMPETING FINANCIAL INTERESTS

The authors declare no competing financial interests.

Europe PMC Funders Author Manuscripts

Molecular-based functional materials can allow the exploitation of the richness of molecular structures to implement in technology novel and unexpected properties. Among the next-generation sensors, transistors, and memory devices, those based on spin state of molecules represent promising alternatives to traditional technologies.[1,2] In this context there is a keen interest on Single-Molecule Magnets (SMMs),[3] functional molecules featuring magnetic memory at the single molecule scale[4,5] as well as quantum effects.[6-9] However, beyond temperature limitations, a quick development of a *SMM-based technology* is hampered by the intrinsic chemical fragility of most polynuclear SMMs and the evanescence of the SMM behaviour, which make the retention of the molecular magnetic bistability at the nanoscale far from trivial. The chemical bond between a sulphur functionalised tetrairon(III) SMM, Fe_4, and a gold surface has been recently employed and the typical magnetic hysteresis observed through synchrotron-light based experiments.[10,11] However, the lability of the Au-S bond[12] cannot guarantee the long term stability required for the development of an SMM-based device. For this reason grafting of SMMs on a particularly attractive inorganic platform such as silicon wafers, offer the possibility to make robust and durable devices by forming stable Si-C covalent bonds. Moreover, the possibility of different doping of the silicon substrate can be used to influence the electronic properties of the grafted molecules[13] and the mobility of the charge carriers in the final hybrid device. Although preliminary promising results have been obtained with Fe_4 SMMs chemically anchored on silicon,[14] the very low temperature required for the observation of magnetic bistability (below 1K) has prompted us to another molecule, that is the Terbium(III) bis(phthalocyaninato) neutral complex,[15] $TbPc_2$ hereafter. Slow dynamics in the magnetisation reversal is here due to the large activation energy barrier generated by crystal field splitting of the J=6 ground multiplet of the highly anisotropic Tb^{III} ion.[16] This results in one of the most promising and widely investigated SMMs,[17-22] the insertion of which in single molecule transport devices, has allowed to monitor the quantum dynamics of a single nuclear spin[23] and to observe a novel supramolecular spin valve effect.[24] In general, however, the magnetisation dynamics of $TbPc_2$ is severely altered in amorphous materials, where the packing of the molecules characterising the crystalline phase is lost.[25,26] The origin of the phenomenon remains unclear, although it should be considered that small distortion of the two phthalocyaninato ligands from the perfectly staggered configuration, corresponding to D_{4d} symmetry, can be very efficient in promoting the tunnel mechanism of relaxation.[26] A similar reduction of the magnetic bistability is observed at the nanoscale: by thermal evaporation of these double-deckers on clean metallic surfaces in Ultra-High Vacuum (UHV) environment the wide opening of the magnetic hysteresis loop above liquid helium temperature vanishes.[27,28] The phthalocyaninato ligands appear to efficiently couple the magnetic moment of the Tb ion with the magnetisation of substrates as recently shown for submonolayer UHV-prepared deposits of $TbPc_2$ on magnetic substrates.[29,30] The strength of the interaction can be tuned by modifying the electronic characteristics of the substrate, though also in these cases no evidence of the SMM character of the pristine molecular system has been observed.

Here we report the outcome of an alternative approach aimed at the exploitation of the magnetic bistability of double-decker systems in a robust nanostructure, prerequisite to fruitfully benefit from SMM features in *ad hoc* designed molecular devices. This has been achieved by the functionalisation of the original $TbPc_2$ system, resulting in a homoleptic

Europe PMC Funders Author Manuscripts

double decker derivative bearing long aliphatic chains with terminal double bonds that allow the grafting of the molecule to the silicon surface from a diluted solution. By using X-ray Circular Magnetic Dichroism to extract the magnetic properties at the nanoscale, with the support of other parallel chemical and structural characterisations flanked by theoretical analysis we demonstrate that SMM behaviour with enhanced hysteresis is retained on a partially ordered and chemically robust monolayer of molecules grafted on Si(100) surface through hydrosilylation reaction.

RESULTS

Synthesis of the $TbPc_2(OC_{11}H_{21})_8$ complex

Silicon was chosen as surface for grafting because of its technological relevance and for the possibility to form thermally and hydrolytically stable Si-C bonds via thermal hydrosilylation.[31] The design of a suitable $TbPc_2$ for silicon grafting requires the introduction of ω-functionalised alkyl chains at peripheral positions of the phthalocyanine ligands. The classical De Cian synthesis,[32] starting from the Terbium(III) acetylacetonate and 1,2-dicyanobenzene derivatives, has been adopted here. The alternative option of $TbPc_2$ post-functionalisation turned out to be synthetically unfeasible in this case. Moreover, the only substituents compatible with the harsh reaction conditions required for double decker formation were alkoxy derivatives, excluding most of the common linker groups such as esters, amides and carbamates. The required 4-(ω-undecenyloxy)phthalonitrile precursor[33] was synthesised from the commercially available 4-hydroxyphthalonitrile by the addition of 11-bromo-1-undecene in the presence of an excess of potassium carbonate in DMF in 80% yield. Homoleptic **$TbPc_2(OC_{11}H_{21})_8$** was then obtained by heating Terbium(III) acetylacetonate in refluxing 1-hexanol in the presence of 4-(ω-undecenyloxy)phthalonitrile, with 1,8-diazabicyclo[5.4.0]undec-7-ene (DBU) as a basic catalyst (Fig. 1a). The neutral double decker compound was isolated in 35% yield as a mixture of constitutional isomers in the form of dark-green powder (see Methods and Supplementary Note 1).

The resulting **$TbPc_2(OC_{11}H_{21})_8$** was characterised via high resolution MALDI-ToF mass spectrometry, X-ray Photoelectron Spectroscopy (XPS) and UV-Vis spectroscopy (see Fig 1 and Supplementary Note 2). Mass spectrometry, the most employed analytical tool for this class of compounds, revealed a unique peak centred at 2529.44 m/z that corresponds well in position and isotopic distribution to the calculated ones for the molecular ion of **$TbPc_2(OC_{11}H_{21})_8$** (Fig. 1b and inset). The UV-VIS spectrum of **$TbPc_2(OC_{11}H_{21})_8$** recorded in chloroform solution shown in Fig. 1c, confirms the neutral π radical form of the molecule: the spectrum exhibits the characteristic absorption bands of double decker phthalocyaninato complexes.[34] The Q band at 681 nm results from the promotion of an electron from the first semi-occupied molecular orbital (SOMO) to the second lowest unoccupied molecular orbital (LUMO) and from the second fully occupied highest occupied molecular orbital (HOMO) to the first LUMO. Furthermore the spectrum shows a typical split Soret-band, resulting from the electronic transitions from the third occupied HOMO to the first LUMO, with maxima at 329 and 361 nm. The two weak π-radical bands at 469 nm and 926 nm are due to electronic transitions from the SOMO orbital to the degenerate LUMOs. The multiplicity associated to the several isomers of **$TbPc_2(OC_{11}H_{21})_8$** produced

in the reaction does not allow the univocal attribution of all resonances by NMR (Supplementary Fig. 1). However, the strong paramagnetic upfield shifts at negative ppm are indicative of Tb complexation even if the presence of these paramagnetic units hampers a proper spectral assignment of the aromatic protons.

XPS spectra of a reference bulk phase have been recorded on a thick film prepared by drop casting a diluted dichloromethane solution of the complexes on a polycrystalline gold substrate. A semi-quantitative analysis of the spectra (Supplementary Fig. 2 and Supplementary Table 1) reveals an atomic composition of the compound in agreement, within the limits of the technique, with the proposed formula, thus confirming the mass spectrometry results.

Magnetic characterisation of bulk $TbPc_2(OC_{11}H_{21})_8$

Magnetic characterisation, performed with standard AC and DC magnetometric techniques (Fig. 2, Supplementary Fig. 3) clearly indicates the SMM behaviour of the complex in its bulk phase. In zero static field the AC susceptibility *vs* temperature curves are characterised by a frequency dependent peak in the out-of-phase component occurring at relatively high temperatures, e.g. the maximum in χ" at 1 kHz is observed at 47 K, which well compares with those reported for similar homoleptic substituted $TbPc_2$ systems.[35] A more careful analysis of the frequency dependence of the AC susceptibility in a wide frequency range, 0.5 Hz - 10 kHz, was performed with the extended Debye model[3] allowing to extract the relaxation time, τ and its distribution width through the empirical parameter, α (Supplementary Note 3). The temperature dependence of τ is shown in Fig. 2b. A linear behaviour in the $\ln(\tau)$ *vs.* $1/T$ plot is observed at zero static field in the high temperature regime, $T > 35$ K, providing the parameters $\tau_0 = 5.5\pm0.7\times10^{-12}$ s and $\Delta/k_B = 811\pm5$ K for the best fit with the Arrhenius law, $\tau = \tau_0 \exp(\Delta/k_BT)$. The estimated energy barrier in the thermally activated process is smaller than that found for the crystalline phase of $TbPc_2$ (965 K)[35] but it is close to the value observed in similar conditions for amorphous unfunctionalised $TbPc_2$ system (856 K)[26], in agreement with the amorphous character of **$TbPc_2(OC_{11}H_{21})_8$** sample. Below 35 K the relaxation becomes temperature independent, indicating the onset of a tunnel mechanism of relaxation, with a significant increase of the width of the distribution of the relaxation times.

A better simulation of χ" *vs.* ν curves is achieved taking into account the presence of a bimodal distribution, see Supplementary Fig. 4, only the dominating one being reported in Fig. 2b.

The application of a static field of 5 kOe (data in Supplementary Fig 3 and Supplementary Fig. 5) provides comparable high temperature behaviour as shown in Fig. 2b, but significantly affects the magnetic relaxation below 35 K, suppressing the tunnelling mechanism with τ exceeding the accessible timescale of the AC susceptometer (~ 10 s). A single distribution of τ is observed in static field because distortions from idealised D_{4d} symmetry present in this amorphous material are less relevant when resonant quantum tunnelling is suppressed. Magnetisation *vs.* field measurements performed at several temperatures and scanning the field between 30 kOe and −30 kOe at 50 Oe s^{-1} (see Fig. 2c)

evidence the opening of a hysteresis below 15 K with the typical butterfly shape induced by the enhancement of quantum tunnelling in zero applied field.[36]

Monolayer preparation and chemical characterisation

The **$TbPc_2(OC_{11}H_{21})_8$** complex has been anchored on a H-terminated Si(100) surface via thermal hydrosilylation of the double bonds according to published literature.[37] The hydrosilylation reaction leads to the formation of a robust Si-C bond and it occurs by placing the alkene functionalised molecules in a 10^{-3} M mesitylene solution at 200°C in presence of a freshly etched H-terminated Si(100). After grafting, several cycles of cleaning (including the sonication of the sample in several solvents) guarantee the removal of all the physisorbed materials leaving on the surface only the monolayer of grafted molecules. The silicon anchored complex, **$TbPc_2(OC_{11}H_{21})_8$@Si** hereafter, has been characterised by XPS in order to verify the chemical integrity of the system (see Supplementary Note 4); only Tb*3d*$_{3/2}$, N*1s* and C*1s* signals have been included in a semiquantitative estimation of the element content on surface and are reported as Supplementary Information (see Supplementary Fig. 2 and Supplementary Table 1). Even considering the experimental error of XPS and the presence of adventitious carbon contamination in this *ex situ* prepared sample, we can assert that the procedure of grafting assures the deposition of the intact system.

Additional information on the monolayer nature can be obtained by the analysis of the N*1s* peak shape. The comparison between the spectra of the monolayer and that of the thick film, reported in Fig. 3, evidences in fact significant differences. The drop cast film features a unique peak at 398.3 eV arising from the superposition of the contributions from the pyrrole-aza coordinating the metal and from the meso-bridging aza nitrogen atoms, as expected for a metal coordinated phthalocyanine.[38] On the contrary the N*1s* spectral region of the monolayer presents, in addition to this signal, a more intense component at higher energy (400.3 eV), clearly indicating that a modification occurs in the chemisorbed molecules.

Interestingly, we show in Fig. 3c that a similar shift to higher energy of the N*1s* signal can be induced also on a bulk sample of **$TbPc_2(OC_{11}H_{21})_8$** by exposing its solution to chlorine and then preparing a drop cast deposit. The treatment with chlorine, already described in literature for Lutetium(III) bis(phthalocyaninato) exposed to Cl_2 under high vacuum condition,[39] induces the formation of the corresponding cationic double-decker species,[40] i.e. the oxidised complex in which one of the electrons of the bis(phthalocyaninato) ligands shell has been removed.

The fact that this is a surface induced effect is evidenced by experiments where the **$TbPc_2(OC_{11}H_{21})_8$** concentration in the solution grafting was reduced to 10^{-5} M. The XPS analysis (see Supplementary Fig. 6) indicates that the lower surface coverage obtained in these conditions increases the contribution of the higher energy contribution to the N*1s* spectrum. On the basis of these evidences, the energy shift can be inferred to result either from a *stabilization effect* of the cationic species formed during the grafting reaction by the silicon surface or from an *electron depletion* of the molecular system induced by the interaction with the surface, in analogy to similar effects experimentally observed and

discussed for various phthalocyanine monolayers adsorbed on semiconducting oxides[41-43] but never reported for double-decker complexes.

Density functional theory (DFT) calculations (see Supplementary Note 5) have been performed in order to clarify the effect of the oxidation of the double decker systems on the XPS spectra as well as the perturbation due to the silicon surface on the energy of core electrons in the complex. A non periodic cluster approach, adopted to model the silicon surface, proved to be well suited in the perspective to obtain information on the core electron energy trend, even if a perfect reproduction of the experimental data is beyond the purposes of this paper. Results shown in Supplementary Fig. 7 evidence that nitrogen *1s* electrons are dispersed around a single energy value in the neutral double-decker species in the gas phase. Similar findings emerge on the cationic species but the mean value is significantly shifted at higher energy (+2.4 eV) due to the effect of the positive charge on the core electron distribution. Once the double deckers lie in contact with the silicon surface, the nitrogen *1s* electrons remain dispersed around a single energy value in both neutral and cationic species. A small energy shift (+0.1 eV) is observed on the neutral double-decker, whereas a significant shift to lower binding energy is observed for the cationic species as a consequence of the ion pair formation between the positively charged molecule and negatively charged surface, where one oxo-termination has been introduced to respect the charge neutrality. This effect, however, decreases significantly by increasing the Si cluster size used to model the surface (Supplementary Fig. 8), and an accurate estimation of the energy difference between neutral and cationic species on surface cannot be achieved. Nevertheless, these theoretical results confirm our assignement of the observed N*1s* shift to electron depleted $TbPc_2$ species stabilised by the silicon surface.

Structural characterisation of the $TbPc_2(OC_{11}H_{21})_8$@Si monolayer

Linear and circular polarisation dependent X-ray absorption experiments have been carried out on the **$TbPc_2(OC_{11}H_{21})_8$@Si** monolayer in order to evaluate with the highest level of accuracy the structural and magnetic properties of the assembled nanostructure. Actually the element selectivity of this synchrotron based technique guarantees addressing directly the properties of the anchored molecules by focusing the measurements at the Tb $M_{4,5}$ absorption edges, while the surface sensitivity is warranted by the adopted detection mode, i.e. the Total Electron Yield (TEY) mode.[44] Moreover the DEIMOS beamline, located at Synchrotron SOLEIL (France), has been specifically designed to carry such measurements: very high beam stability combined with reduced photon flux guarantee measurements reproducibility without damaging the samples.[45]

At first, X-ray Natural Linear Dichroism (XNLD) has been measured for the $M_{4,5}$ Tb edges. The sample has been set so that the normal to the surface **n** and the X-ray propagation vector **k** lie in the horizontal plane with (**n**,**k**) = 60°. The cross-sections with horizontal linear polarisation (σ_H) and with vertical linear polarisation (σ_V) have been measured (See Figure 4a and Supplementary Figure 9).

In the ideal case where $TbPc_2$ molecules adopt a *lying down* configuration, i.e. the phthalocyaninato C_4 axis is parallel to the surface normal, the electric field of the vertically polarised light is aligned perpendicular to the symmetry axis of the coordination square

antiprism of the Tb^{III} ion, while the horizontal one forms an angle of 30° with this axis. In the opposite case, where $TbPc_2$ molecules adopt a standing configuration with no order in the plane, the electric field of the vertically polarised light can be now aligned at any angle with the symmetry axis of the molecules, while for the horizontal polarisation the electric field cannot be parallel to the molecular symmetry axis. It is thus straightforward, that XNLD, evaluated as ($\sigma_V - \sigma_H$), changes sign for the two configurations and can therefore be employed to extract information on the molecular arrangement in the monolayer.

By the comparison (see Supplementary Note 6) with experimental and theoretical reports from earlier literature[27] it can be straightforwardly assessed that the molecules forming the monolayer are preferentially oriented with a *lying down* configurations, with the oriented molecules accounting for about half of the sample. It is interesting to notice that a reversed XNLD signal is measured in a bulk sample obtained by drop casting a solution of **$TbPc_2(OC_{11}H_{21})_8$** (see Supplementary Fig. 10). This finding is in line with the common tendency for thick bis(phthalocyaninato) films to aggregate in a *standing up* configuration,[27] and the observed difference between the two samples confirms that our monolayer of $TbPc_2$ does not contain physisorbed aggregates.

Magnetic characterisation of the $TbPc_2(OC_{11}H_{21})_8$@Si monolayer

X-ray absorption experiments carried out at low temperature, under a 50 kOe magnetic field parallel to the X-ray light propagation vector, using circularly polarised light allowed to extract also the X-ray Magnetic Circular Dichroism (XMCD). This is defined as the difference ($\sigma^- - \sigma^+$) between the absorption spectra obtained with right (σ^-) and left (σ^+) polarised light. The result for the monolayer is reported in Fig. 4b: detected features and the intensity of the dichroic signal are in line with the expected ones[27,28] for a saturated Tb^{3+} system characterised by total angular momentum $J=L+S=6$.

Fig. 5a reports the variation of the XMCD contribution at the M_5 edge, normalised to the saturation value, as a function of the applied magnetic field between −50 kOe and 50 kOe at three different temperatures. We stress here that, profiting from the fast TEY detection setup and the stability of the experimental apparatus developed in the DEIMOS beamline,[45] it has been possible to collect the signal as a function of the fast sweeping field, thus providing highly resolved XMCD-detected magnetisation curves clearly showing hysteretic behaviour already at 4.3 ± 0.2 K.

The opening of the hysteresis strongly depends on the temperature and also on the speed of the scanning field (see Supplementary Fig. 11), confirming the dynamic character of the magnetic bistability typical of $TbPc_2$ SMMs. A tiny angular dependence of the hysteresis is also detected (see Fig. 5b and Supplementary Fig. 11) in line with the XNLD indications of a partial orientation of the molecular film. Most important is that the comparison with the behaviour of the bulk phase (see Fig. 2c, and Supplementary Fig. 12 for a direct comparison at the same field scan rate) reveals a significantly larger opening of the hysteresis for the monolayer. To further investigate this aspect an analogous XMCD characterisation has been carried out on the drop cast thick film of **$TbPc_2(OC_{11}H_{21})_8$**, evidencing an opening on the hysteresis cycle significantly weaker than in the monolayer grafted to the Si surface (see Fig. 5b), in line with standard magnetometry experiments on the pristine compound.

A better estimation of the changes in the hysteretic behaviour can be achieved by plotting the difference in the magnetisation obtained for increasing and decreasing field: $\Delta M(H) = |M(H\uparrow) - M(H\downarrow)|$

The area under these curves (Fig. 5c) thus corresponds to the opening of the hysteresis loop, which results to be significantly larger in the monolayer sample than in the thick film. A similar enhancement of the bistable behaviour in the monolayer is also observed for hysteresis curves taken at different orientation of the substrate in respect to the magnetic field (Fig. 5 and Supplementary Fig. 11 for more data), thus indicating that the observed phenomenon is not due to orientation effects but has to be related to the grafting process.

DISCUSSION

The profusion of experiments performed on the $TbPc_2$ family of SMM has revealed significant changes in the magnetic bistability depending on the nature of the substrate the SMM is deposited onto. The mechanism of these modifications remains however obscure. With metallic substrates the typical butterfly hysteresis observable well above helium temperature disappears, though pyrene-functionalised $TbPc_2$ when grafted to single wall carbon nanotubes exhibits an increase of the remnant magnetisation at sub-kelvin temperatures[46] that is the opposite of the trend observed when other SMM are grafted to carbon nanotubes.[47] When ferromagnetic substrates are employed the $TbPc_2$ hysteresis is observed at much higher temperatures[29] but the bistability and coercivity are those of the substrate and cannot be considered an intrinsic property of the single molecule. We notice that an enhancement of the opening of the hysteresis has been observed[40] at 1.5 K in frozen solution by oxidation of the double decker to the cationic $[TbPc_2]^+$ species, an effect that seems further enhanced in the monolayer investigated here.

The use of silicon, unprecedented for this type of SMMs, presents several interesting advantages. Our results show that $TbPc_2$ SMMs can be covalently and robustly anchored to a silicon substrate, with the deposited monolayer standing harsh treatments like sonication in dichloromethane. Si-C covalent bonds in fact guarantee a higher stability respect to π-stacking or S-Au interactions. Moreover, the pronounced magnetic bistability not only is retained at the level of the monolayer but, when quantified as the area enclosed in the hysteresis cycle, it happens to be significantly enhanced by the grafting process to silicon, even if with small remnant magnetisation. More important is that this alteration correlates with changes observed in the photoelectron spectra. Though the long alkyl chains in this Tb double decker SMM could in principle hamper a significant interaction with the substrate, their flexibility, as already observed for functionalised $TbPc_2$ molecules grafted on gold[48] induces a preferential lying down configuration that can allow a stabilisation of an oxidised $TbPc_2$ system by the silicon substrate as indicated by coverage dependent XPS results. It is well known that the oxidation of the Pc ligands reduces the height of the square-antiprism coordination polyhedron with a sensible enhancement of the effective energy barrier for the reversal of the magnetisation and more pronounced hysteretic behaviour.[15,16,49] Covalent grafting to the silicon surface appears to have a similar effect on the electron density of the phthalocyanine rings and is therefore not unreasonable that it can equally affect the magnetic

Europe PMC Funders Author Manuscripts

anisotropy of the complex, enhancing the magnetic bistability though not preventing tunnelling in zero field.

In conclusion, our XMCD observation of the enhanced magnetic hysteresis evidences that a careful choice of the substrate and of the grafting strategy can be exploited to tune the electronic properties of these SMMs and optimise their magnetic behaviour, in contrast to what has been observed by assembling the pristine $TbPc_2$ system on solid surfaces by thermal evaporation procedures in UHV.[27,29,30,50,51] The chemical robustness of these covalently grafted monolayers make them suitable for insertion in spintronic devices prepared by solution techniques, which is the emerging trend in this rapidly evolving field.[52]

METHODS

Synthesis of $TbPc_2(OC_{11}H_{21})_8$

To a stirred solution of 4-(ω-undecenyloxy)phthalonitrile (**2**) (400.0 mg, 1.35 mmol, see Supplementary Note 1) in 1-hexanol (8 mL) $[Tb(acac)_3]\cdot nH_2O$ (98.6 mg, 0.216 mmol, 0.16 equiv) was added followed by 1,8-Diazabicyclo[5.4.0]undec-7-ene (DBU) (202.0 μL, 1.35 mmol, 1 equiv). The reaction was heated to reflux and stirred for 16 h. The dark-green mixture was cooled to room temperature and the solvent removed under reduced pressure. Methanol was added to the residue until a precipitate formed. The green finely dispersed mixture was filtered off and purified by flash chromatography ($CHCl_3$ as eluent) to obtain a green solid (149.2 mg, 35% yield). UV/Vis: λ_{max} ($CHCl_3$) 926, 681, 469, 361, 329 nm; MALDI-TOF: $[M]^+$calculated for $C_{152}H_{192}N_{16}O_8Tb$, 2529.439 m/z; found, 2529.444 m/z.

Magnetic characterisation of the bulk system

Quantum Design PPMS Vibrating Sample Magnetometer (VSM) set-up in the continuous measurement mode sweeping the magnetic field at 50 $Oe\cdot s^{-1}$ was used to characterise a bulk $\mathbf{TbPc_2(OC_{11}H_{21})_8}$ sample, pressed in a pellet, between −50 kOe and 50 kOe. AC magnetic susceptibility up to 10 kHz of this sample was measured with the same Quantum Design PPMS platform in zero and 5 kOe static fields. Quantum Design MPMS SQUID magnetometer was employed to extend the AC susceptibility measurements in the low frequency range (down to 0.1 Hz).

Monolayer preparation

The $\mathbf{TbPc_2(OC_{11}H_{21})_8}$ solutions in mesitylene, were placed in a small, three-necked flask fitted with a nitrogen inlet and a condenser. The solutions were deoxygenated with dry nitrogen for at least 1 h. Subsequently, *p*-doped Si(100) (Boron doped, resistivity 1.5-4 Ω cm) substrates were treated in a piranha solution for 12 min, rinsed in water for 2 min, and etched in 1.0% hydrofluoric acid for 90 s, then immediately placed in the alkenes solution. The solutions were then refluxed at 200 °C for 2 h, under slow N_2 bubbling to prevent bumping. After cooling to RT, the samples were removed from the flask and cleaned by several rinsing cycles of ultrasonic cleaner.

XPS measurements

XPS spectra of the monolayer of **$TbPc_2(OC_{11}H_{21})_8$@Si** were run with a PHI 5600 multitechnique ESCA-Auger spectrometer equipped with a monochromatic Al Kα X-ray source. Analyses were carried out with an analyser pass energy of 23.5 eV and a photoelectron angle of 45° (relative to the sample surface) with an acceptance angle of ±7°. Bulk drop cast and Cl_2 - treated **$TbPc_2(OC_{11}H_{21})_8$** sample have been measured with a VSW setup equipped with non monochromatic Al Kα source not focalised; in this case the angle between the analyser axis and the X-ray propagation vector from the X-ray source was 54.44° and a pass energy of 44 eV was used. These different conditions were required to properly characterise these samples avoiding the reduction of the oxidised system by the effect of the photo-electrons and secondary electrons. In all spectra, XPS binding energy scale was calibrated by placing the C*1s* peak due to hydrocarbon moieties and "adventitious" carbon at 285.0 eV. Data analysis was performed using a mixed Gaussian and Lorentzian line-shape and background subtraction using a Shirley function. The elemental composition of the samples was evaluated by estimating the integrated area of each component corrected for the corresponding photo-ionisation cross-section.[53] The Tb$3d_{3/2}$ sensitivity factor was empirically verified from terbium(III)acetate hydrate powder (see Supplementary Fig. 13).

X-ray Absorption Spectroscopy measurements

X-ray absorption spectroscopy and XMCD spectra at the Tb $M_{4,5}$ edges were recorded at the DEIMOS beamline,[44] Synchrotron SOLEIL facility in France on a UHV compatible pumped ^{4}He cryo-magnet. Absorption spectra were measured in Total-Electron Yield (TEY) detection mode to guarantee the optimal detection sensitivity. All the characterisations were performed using a low density of photons in order to avoid radiation damages.

XNLD experiments were carried out by recording XAS with linearly polarised light (vertical and horizontal polarisation) in a 50 kOe field (to enhance the TEY) placing the normal of sample surface at 60° with respect to the X-ray light propagation vector and extracted as ($\sigma_V - \sigma_H$). Final XNLD spectrum is the result of the averaging of 4 scans per polarisation, for both positive and negative magnetic field in order to avoid contamination from spurious X-ray magnetic linear dichroism (XMLD) signal.

XMCD spectra were obtained with a similar averaging procedure[54] from circularly polarised (left and right) absorption spectra measured at the temperature of 2 K and under an applied magnetic field of 50 kOe parallel to the X-ray propagation vector. The same set-up was used to record the XMCD dependence on the magnetic field (hysteresis curves) as a function of sample orientation and temperature, as well as field sweeping rate. Data have been normalised with respect to the saturation value in order to be able to compare this experiment with traditional magnetometry experiments and evaluate the angular dependence.

DFT calculations

Calculations were performed adopting the Perdew, Burke and Ernzerhof (PBE) formalism for both exchange and correlation functionals.[55] The effective core potential (ECP) of Hay

and Wadt[56] were used for the yttrium and terbium atoms. The standard all-electron 6-31G** basis was used for all remaining atoms.[57] Closed or open shell approach are adopted depending on the charge state of the double decker system we considered: for a +1 charged system a closed shell is adopted whereas for the neutral bis-phthalocyaninato system an open shell is adopted to take into account the electron multiplicity. Si(100) surface was represented by a cluster of 21 silicon atoms H-terminated with one hydroxyl termination. Moving from the gas phase to the surface absorbed molecules, $TbPc_2$ was replaced by YPc_2 to avoid convergence complication due to the high multiplicity arising from *f* electrons of the terbium atom (see Supplementary Note 5 for further details). Molecular geometry optimization of stationary points was carried out without symmetry constrains and was based on an analytical gradient minimisation approach. All calculations were performed using NWCHEM code[58] on Linux cluster systems.

Supplementary Material

Refer to Web version on PubMed Central for supplementary material.

ACKNOWLEDGEMENTS

We thank the staff of the DEIMOS beamline including Loic Joly, Bernard Muller and Jean-Paul Kappler for the development of the facilities available at the beamline and the interdepartmental Centre SITEIA.PARMA, University of Parma for mass spectrometry measurements. Funding from the European Research Council through the Advanced Grant “MolNanoMas” (267746), EC through from FP7 project “FINELUMEN” (FP7-PEOPLE-2007-1-1-ITN215399) and the Italian MIUR through FIRB projects “NanoPlasMag” (RBFR10OAI0) and “Nanomagneti molecolari su superfici metalliche e magnetiche per applicazioni nella spintronica molecolare” (RBAP117RWN) and the PRIN project “RECORD” (20097X44S7) are acknowledged. Instrumental investments on DEIMOS have been provided by IMPMC-UMR7590 through ANR-07-BLANC-0275. A. M. acknowledges CINECA Award N. HP10C9RDDE 2013 for providing high performance computing resources and support.

REFERENCES

1. Aviram A, Ratner MA. Molecular rectifiers. Chem. Phys. Lett. 1974; 29:277–283.
2. Aradhya SV, Venkataraman L. Single-molecule junctions beyond electronic transport. Nat. Nanotechnol. 2013; 8:399–410. [PubMed: 23736215]
3. Gatteschi, D.; Sessoli, R.; Villain, J. Molecular Nanomagnets. Oxford University Press; USA: 2006.
4. Sessoli R, Gatteschi D, Caneschi A, Novak MA. Magnetic bistability in a metal-ion cluster. Nature. 1993; 365:141–143.
5. Christou G, Gatteschi D, Hendrickson DN, Sessoli R. Single-Molecule Magnets. Mater. Res. Bull. 2000; 25:66–71.
6. Thomas L, et al. Macroscopic quantum tunneling of magnetization in a single crystal of nanomagnets. Nature. 1996; 383:145–147.
7. Friedman JR, Sarachik MP, Tejada J, Ziolo R. Macroscopic Measurement of Resonant Magnetization Tunneling in High-Spin Molecules. Phys. Rev. Lett. 1996; 76:3830–3833. [PubMed: 10061120]
8. Wernsdorfer W, Sessoli R. Quantum Phase Interference and Parity Effects in Magnetic Molecular Clusters. Science. 1999; 284:133–135. [PubMed: 10102810]
9. Takahashi S, et al. Decoherence in crystals of quantum molecular magnets. Nature. 2011; 476:76–79. [PubMed: 21775988]
10. Mannini M, et al. Magnetic memory of a single-molecule quantum magnet wired to a gold surface. Nat. Mater. 2009; 8:194–197. [PubMed: 19182788]
11. Mannini M, et al. Quantum tunnelling of the magnetization in a monolayer of oriented single-molecule magnets. Nature. 2010; 468:417–421.

12. Schlenoff JB, Li M, Ly H. Stability and Self-Exchange in Alkanethiol Monolayers. J. Am. Chem. Soc. 1995; 117:12528–12536.
13. Woodruff DN, Winpenny REP, Layfield RA. Lanthanide single-molecule magnets. Chem. Rev. 2013; 113:5110–5148. [PubMed: 23550940]
14. Condorelli GG, et al. Site-specific anchoring of tetrairon(III) single molecule magnets on functionalized Si(100) surfaces. Chem. Mater. 2008; 20:2405–2411.
15. Ishikawa N, et al. Upward temperature shift of the intrinsic phase lag of the magnetization of Bis(phthalocyaninato)terbium by ligand oxidation creating an $S = 1/2$ spin. Inorg. Chem. 2004; 43:5498–5500. [PubMed: 15332799]
16. Ishikawa N, et al. Determination of ligand-field parameters and *f*-electronic structures of double-decker bis(phthalocyaninato)lanthanide complexes. Inorg. Chem. 2003; 42:2440–2446. [PubMed: 12665381]
17. Katoh K, et al. Direct Observation of Lanthanide(III)-Phthalocyanine Molecules on Au(111) by Using Scanning Tunneling Microscopy and Scanning Tunneling Spectroscopy and Thin-Film Field-Effect Transistor Properties of Tb(III)- and Dy(III)-Phthalocyanine Molecules. J. Am. Chem. Soc. 2009; 131:9967–9976. [PubMed: 19569681]
18. Komeda T, et al. Observation and electric current control of a local spin in a single-molecule magnet. Nat. Commun. 2011; 2:217. [PubMed: 21364556]
19. Vitali L, et al. Electronic Structure of Surface-Supported Bis(Phthalocyaninato) Terbium(III) Single Molecular Magnets. Nano Lett. 2008; 8:3364–3368. [PubMed: 18800852]
20. Schwöbel J, et al. Real-space observation of spin-split molecular orbitals of adsorbed single-molecule magnets. Nat. Commun. 2012; 3:953. [PubMed: 22805560]
21. Fu Y-S, et al. Reversible chiral switching of bis(phthalocyaninato) terbium(III) on a metal surface. Nano Lett. 2012; 12:3931–3935. [PubMed: 22779916]
22. Gonidec M, et al. Surface Supramolecular Organization of a Terbium(III) Double-Decker Complex on Graphite and its Single Molecule Magnet Behavior. J. Am. Chem. Soc. 2011; 133:6603–6612. [PubMed: 21486019]
23. Vincent R, Klyatskaya S, Ruben M, Wernsdorfer W, Balestro F. Electronic read-out of a single nuclear spin using a molecular spin transistor. Nature. 2012; 488:357–360. [PubMed: 22895342]
24. Urdampilleta M, Klyatskaya S, Cleuziou J-P, Ruben M, Wernsdorfer W. Supramolecular spin valves. Nat. Mater. 2011; 10:502–506. [PubMed: 21685902]
25. Hofmann A, et al. Depth-Dependent Spin Dynamics in Thin Films of $TbPc_2$ Nanomagnets Explored by Low-Energy Implanted Muons. ACS Nano. 2012; 6:8390–8396. [PubMed: 22917162]
26. Malavolti L, et al. Erratic magnetic hysteresis of $TbPc_2$ molecular nanomagnets. J. Mater. Chem. C. 2013; 1:2935–2942.
27. Margheriti L, et al. X-ray detected magnetic hysteresis of thermally evaporated terbium double-decker oriented films. Adv. Mater. 2010; 22:5488–5493. [PubMed: 20949539]
28. Biagi R, et al. X-ray absorption and magnetic circular dichroism investigation of bis(phthalocyaninato)terbium single-molecule magnets deposited on graphite. Phys. Rev. B. 2010; 82:224406.
29. Lodi Rizzini A, et al. Coupling Single Molecule Magnets to Ferromagnetic Substrates. Phys. Rev. Lett. 2011; 107:177205. [PubMed: 22107576]
30. Lodi Rizzini A, et al. Exchange biasing single molecule magnets: coupling of $TbPc_2$ to antiferromagnetic layers. Nano Lett. 2012; 12:5703–5707. [PubMed: 23046484]
31. Linford MR, Chidsey CED. Alkyl monolayers covalently bonded to silicon surfaces. J. Am. Chem. Soc. 1993; 115:12631–12632.
32. De Cian A, Moussavi M, Fischer J, Weiss R. Synthesis, structure, and spectroscopic and magnetic properties of lutetium(III) phthalocyanine derivatives: $LuPc_2 \cdot CH_2Cl_2$ and $[LuPc(OAc)(H_2O)_2] \cdot H_2O \cdot 2CH_3OH$. Inorg. Chem. 1985; 24:3162–3167.
33. Görlach B, et al. Synthesis, characterization and HPLC-applications of novel phthalocyanine modified silica gel materials. J. Mater. Chem. 2001; 11:3317–3325.

34. Jiang J, Ng DKP. A decade journey in the chemistry of sandwich-type tetrapyrrolato-rare earth complexes. Acc. Chem. Res. 2009; 42:79–88. [PubMed: 18767871]
35. Ganivet CR, et al. Influence of peripheral substitution on the magnetic behavior of single-ion magnets based on homo- and heteroleptic Tb(III) bis(phthalocyaninato). Chem. Eur. J. 2013; 19:1457–1465. [PubMed: 23197446]
36. Ishikawa N. Single Molecule Magnet With Single Lanthanide Ion. Polyhedron. 2007; 26:2147–2153.
37. Buriak JM. Organometallic Chemistry on Silicon and Germanium Surfaces. Chem. Rev. 2002; 102:1271–1308. [PubMed: 11996538]
38. Lozzi L, Ottaviano L, Santucci S. High resolution XPS studies on hexadecafluoro-copper-phthalocyanine deposited onto Si(7×7) surface. Surf. Sci. 2001; 470:265–274.
39. Bufler J, Ziegler C, Göpel W. Doping effects in thin films of radical phthalocyanines: UPS and conductivity studies. Synth. Met. 1993; 61:127–131.
40. Gonidec M, Davies ES, McMaster J, Amabilino DB, Veciana J. Probing the magnetic properties of three interconvertible redox states of a single-molecule magnet with magnetic circular dichroism spectroscopy. J. Am. Chem. Soc. 2010; 132:1756–1757. [PubMed: 20099818]
41. Palmgren P, et al. Strong Interactions in Dye-Sensitized Interfaces. J. Phys. Chem. C. 2008; 112:5972–5977.
42. Yu S, et al. Inhomogeneous charge transfer within monolayer zinc phthalocyanine absorbed on TiO_2(110). J. Chem. Phys. 2012; 136:154703–154709. [PubMed: 22519339]
43. Mattioli G, Filippone F, Giannozzi P, Caminiti R, Bonapasta AA. Ab initio Theoretical Investigation of Phthalocyanine-Semiconductor Hybrid Systems. Chem. Mater. 2009; 21:4555–4567.
44. Henke B, Liesegang J, Smith S. Soft-x-ray-induced secondary-electron emission from semiconductors and insulators: Models and measurements. Phys. Rev. B. 1979; 19:3004–3021.
45. Ohresser P, et al. DEIMOS: A beamline dedicated to dichroism measurements in the 350-2500 eV energy range. Rev. Sci. Instrum. 2014; 85:013106. [PubMed: 24517744]
46. Kyatskaya S, et al. Anchoring of rare-earth-based single-molecule magnets on single-walled carbon nanotubes. J. Am. Chem. Soc. 2009; 131:15143–15151. [PubMed: 19799421]
47. Giusti A, et al. Magnetic bistability of individual single-molecule magnets grafted on single-wall carbon nanotubes. Angew. Chem. Int. Ed. 2009; 48:4949–52.
48. Glebe U, et al. Self-Assembled Monolayers of Single-Molecule Magnets [Tb{Pc'$(SR)_8$}$_2$] on Gold. Chempluschem. 2012; 77:889–897.
49. Takamatsu S, Ishikawa T, Koshihara S, Ishikawa N. Significant increase of the barrier energy for magnetization reversal of a single-4*f*-ionic single-molecule magnet by a longitudinal contraction of the coordination space. Inorg. Chem. 2007; 46:7250–7252. [PubMed: 17691726]
50. Klar D, et al. Antiferromagnetic coupling of $TbPc_2$ molecules to ultrathin Ni and Co films. Beilstein. J. Nanotechnol. 2013; 4:320–324. [PubMed: 23766956]
51. Malavolti L, et al. Magnetism of $TbPc_2$ SMMs on ferromagnetic electrodes used in organic spintronics. Chem. Commun. 2013; 49:11506–11508.
52. Tatay S, et al. Self-assembled monolayer-functionalized half-metallic manganite for molecular spintronics. ACS Nano. 2012; 6:8753–7. [PubMed: 22947018]
53. Wagner CD, et al. Empirical atomic sensitivity factors for quantitative analysis by electron spectroscopy for chemical analysis. Surf. Int. Anal. 1981; 3:211–225.
54. Sessoli R, Mannini M, Pineider F, Cornia A, Sainctavit P. Magnetism and Synchrotron Radiation: New Trends. 2010; 133:279–311.
55. Perdew JP, Burke K, Ernzerhof M. Generalized Gradient Approximation Made Simple. Phys. Rev. Lett. 1996; 77:3865–3868. [PubMed: 10062328]
56. Hay PJ, Wadt WR. Ab initio effective core potentials for molecular calculations. Potentials for K to Au including the outermost core orbitals. J. Chem. Phys. 1985; 82:299–310.
57. Rassolov VA, Pople JA, Ratner MA, Windus TL. 6-31G* basis set for atoms K through Zn. J. Chem. Phys. 1998; 109:1223–1229.

58. Valiev M, et al. NWChem: A comprehensive and scalable open-source solution for large scale molecular simulations. Comput. Phys. Commun. 2010; 181:1477–1489.

Europe PMC Funders Author Manuscripts

Europe PMC Funders Author Manuscripts

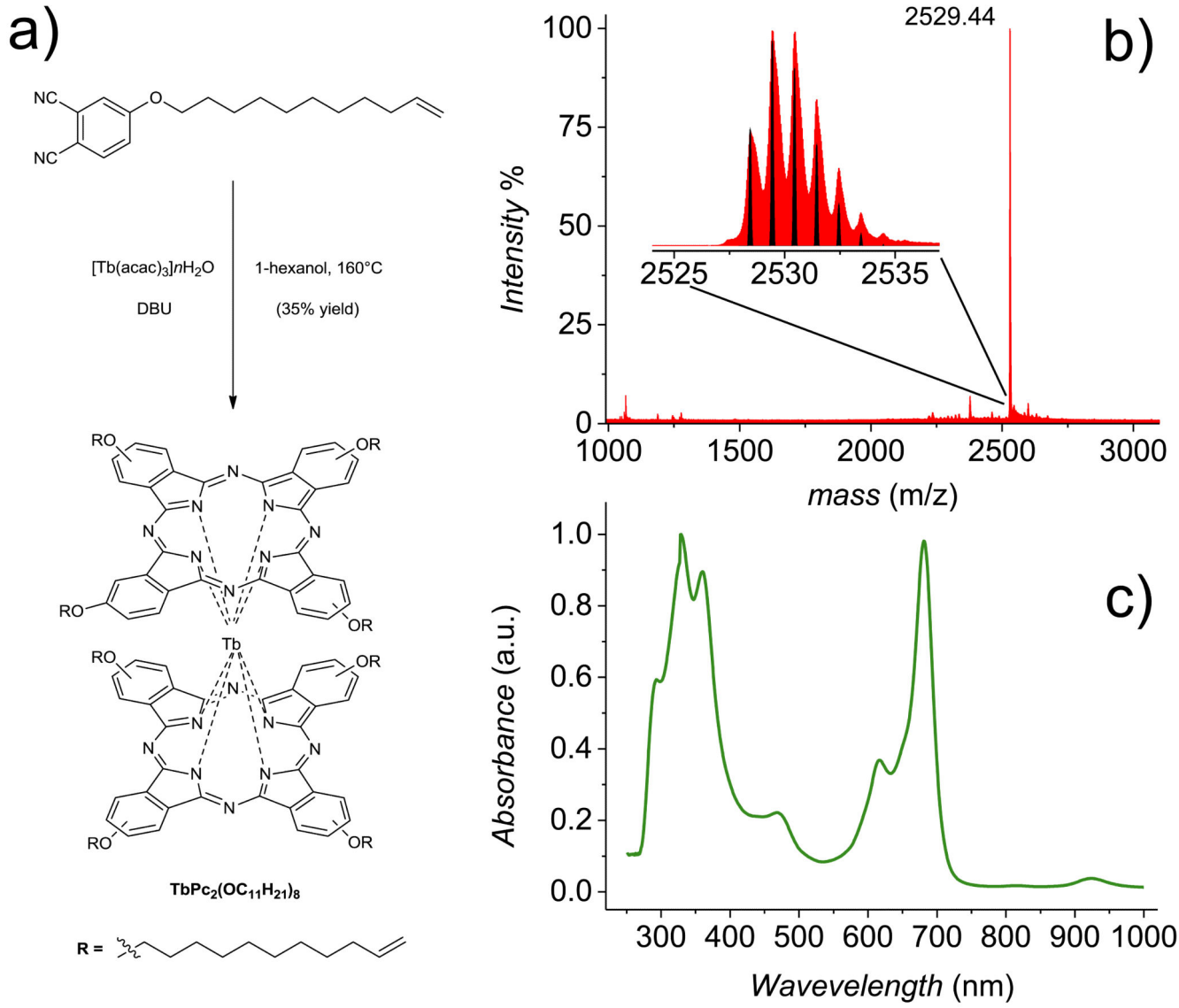

Figure 1. Synthesis and chemical characterization of $TbPc_2(OC_{11}H_{21})_8$

a) Synthesis of homoleptic **$TbPc_2(OC_{11}H_{21})_8$** using 4-(ω-undecenyloxy)phthalonitrile as starting material; *b)* high resolution MALDI-ToF spectrum of **$TbPc_2(OC_{11}H_{21})_8$**, with experimental (red lines) versus theoretical (black) isotopic distribution pattern in the inset; *c)* UV-Vis absorption spectrum of **$TbPc_2(OC_{11}H_{21})_8$** in chloroform.

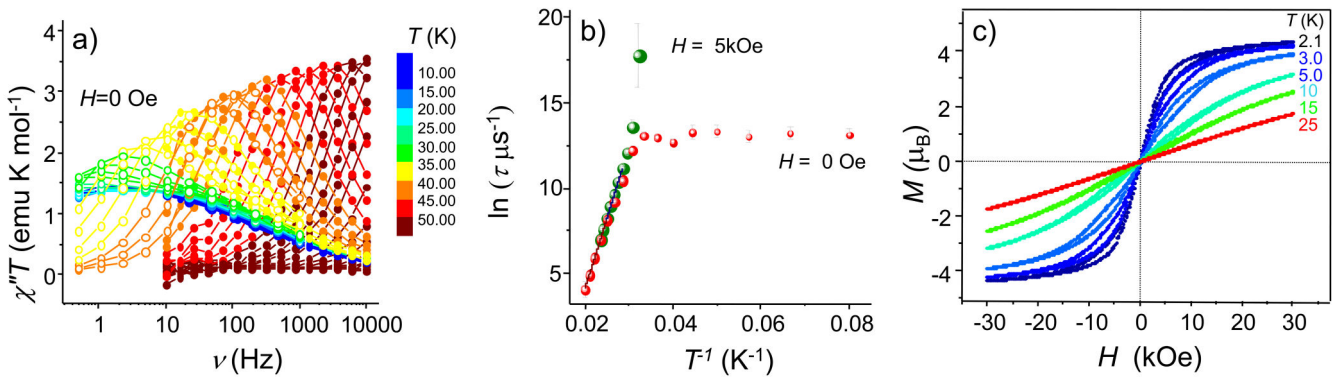

Figure 2. Bulk magnetic properties of $TbPc_2(OC_{11}H_{21})_8$

a) AC susceptibility measurements in zero field. *b)* Arrhenius plot of data extracted from AC measurements in zero field and in a 5kOe static field. *c)* Magnetisation curves as a function of the temperature recorded at a field sweeping rate of 50 Oe s^{-1}.

Europe PMC Funders Author Manuscripts

Europe PMC Funders Author Manuscripts

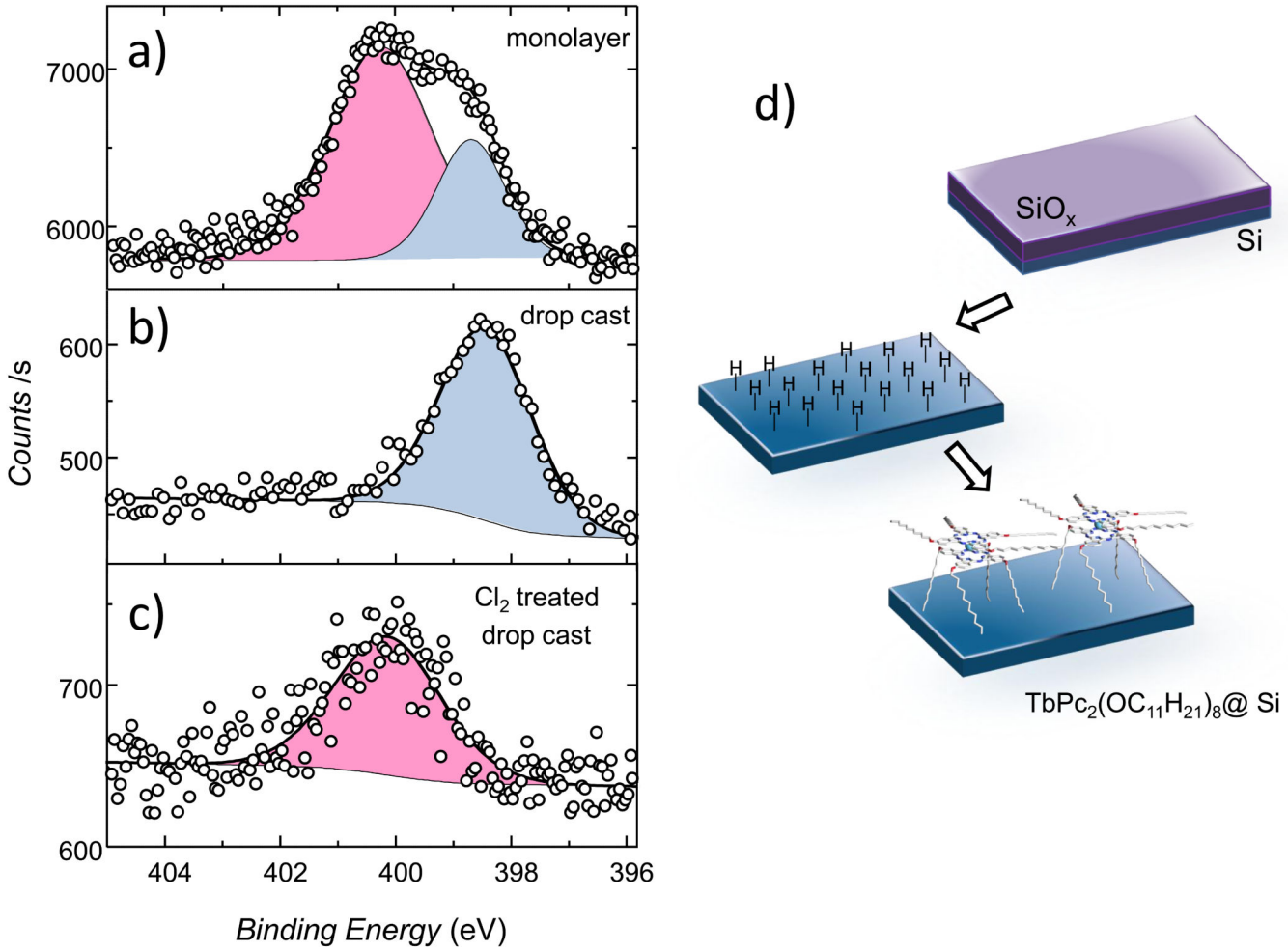

Figure 3. Grafting of $TbPc_2(OC_{11}H_{21})_8$

High-resolution N *1s* XPS spectra of *a)* the **$TbPc_2(OC_{11}H_{21})_8$@Si** monolayer, *b)* the drop cast deposit **$TbPc_2(OC_{11}H_{21})_8$** and *c)* the drop cast sample treated with chlorine. *d)* Sketch of the **$TbPc_2(OC_{11}H_{21})_8$@Si** grafting procedure: *step 1)* etching in 1.0% hydrofluoric acid of silicon surface; *step 2)* hydrosilylation at 200°C for 2h.

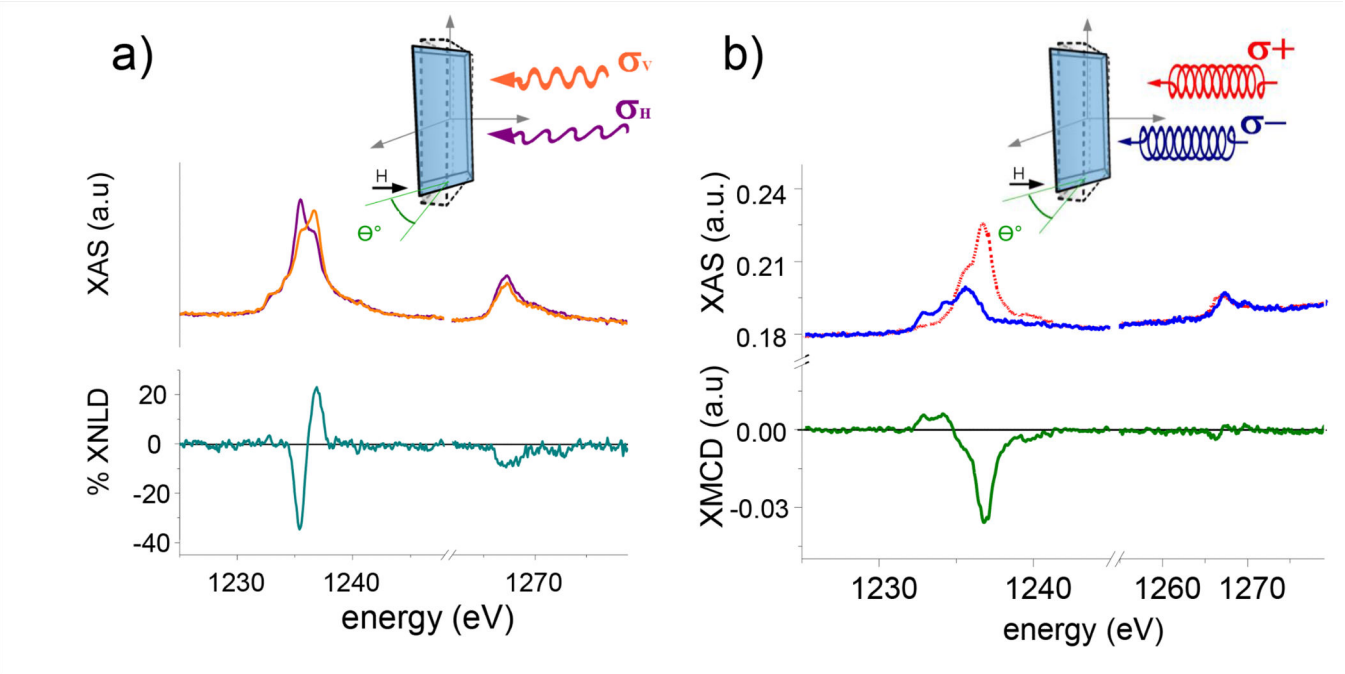

Figure 4. X-ray polarized light absorption

XNLD *(a)* and XMCD *(b)* measurements at 2.2 ± 0.2 K, 50kOe, for (**n**,**k**) = 60°. In the inset the geometry of the two experiments are presented: in a XNLD experiment vertical (σ_V) and horizontally (σ_H) polarised light are used and the sample is rotated by an angle θ between the normal to the surface and the X-ray light propagation direction, an external magnetic field is used only to enhance the TEY detection capabilities; in XMCD experiment light with opposite circular polarization, σ^+ and σ^-, is employed in an analogous experimental geometry, external magnetic field and θ are varied to extract additional information.

Europe PMC Funders Author Manuscripts

Europe PMC Funders Author Manuscripts

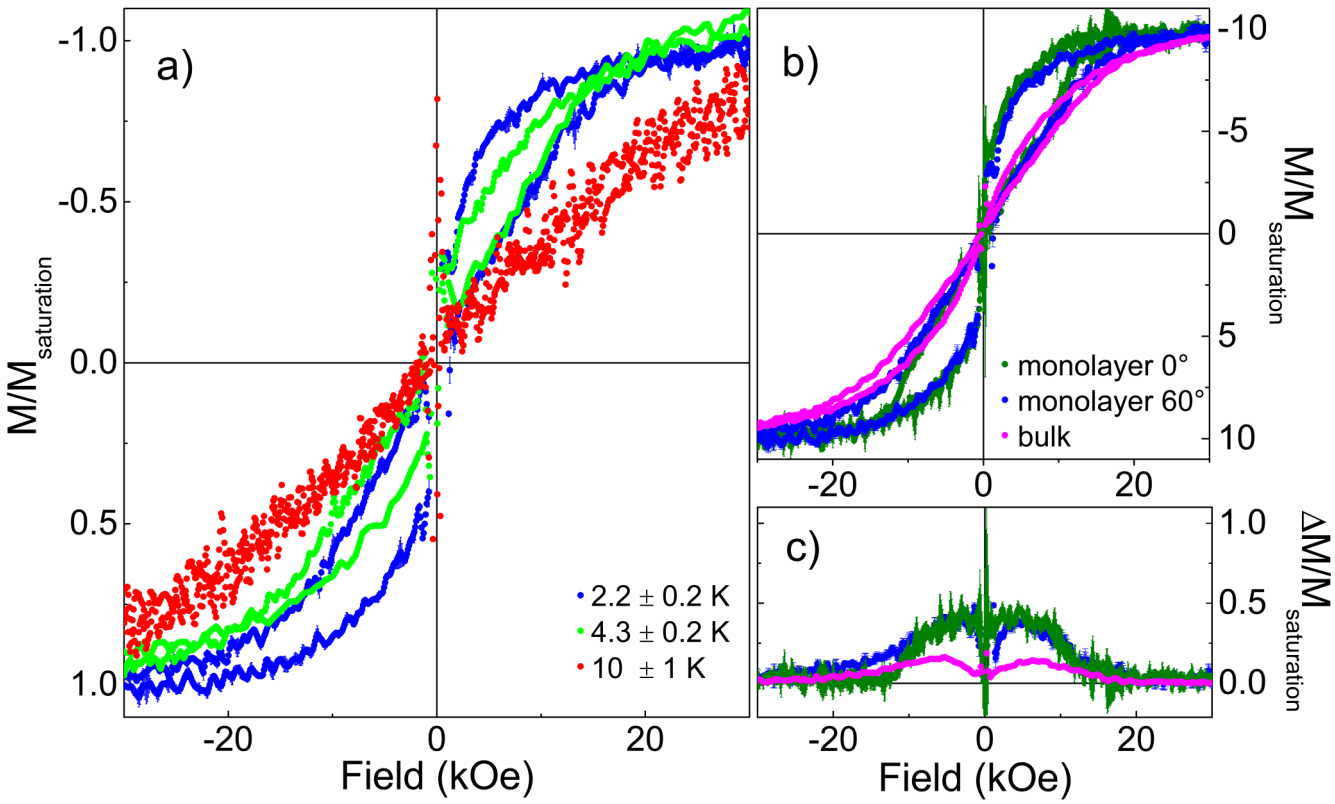

Figure 5. $TbPc_2(OC_{11}H_{21})_8$@Si hysteresis

a) XMCD-detected magnetisation curves for (**n**,**k**) = 60° as a function of the temperature in the **$TbPc_2(OC_{11}H_{21})_8$@Si** monolayer. *b-c)* Comparison between the behaviour of the thick film and the monolayer, the latter being measured for (**n**,**k**) = 0° and 60°. These magnetisation curves, measured in the same condition for all the samples (2.2 ± 0.2 K and 500 Oe s^{-1} scan speed) through the XMCD technique, are reported in figure *b)* with their experimental error. In *c)* the hysteresis opening is estimated as ΔM(H) according to the procedure described in the text.